Polarimetric Decomposition With an Urban Area Descriptor for Compact Polarimetric SAR Data

Qiang Yin, *Member, IEEE*, Jie Xu, Deliang Xiang, *Member, IEEE*, Yongsheng Zhou, *Member, IEEE*, and Fan Zhang, *Senior Member, IEEE*

***Abstract*—The compact polarimetric (CP) synthetic aperture radar (SAR) can alleviate the drawbacks of the fully polarimetric (FP) SAR and provide more target information as compared to the conventional single polarimetric and dual polarimetric mode. However, the present decomposition methods for CP SAR have the problem of overestimation of volume scattering (OVS) among urban areas, especially the obliquely oriented buildings (OOBs). The OVS can cause considerable OVS which leads to the misinterpretation of the scattering mechanism. In this article, a new descriptor of OOBs for the CP SAR is introduced to reduce the volume scattering in the urban areas. And a new model-based decomposition method, which is applicable for both the $\pi/4$ mode and the circular transmit and liner receive mode, is proposed based on the descriptor. The Radarsat-2 FP SAR data are used to simulate the CP SAR data to validate our algorithm. The proposed method improves the double-bounce scattering component in different types of urban areas by about 10%.**

***Index Terms*—Circular transmit and liner receive (CTLR) mode compact polarimetric (CP) synthetic aperture radar (SAR), overestimation of volume scattering, three-component decomposition, $\pi/4$ mode CP SAR.**

I. Introduction

FULLY polarimetric (FP) synthetic aperture radar (SAR) is acknowledged as providing satisfactory performance in SAR applications, due to the complete radar target information content. However, FP SAR systems transmit and receive both horizontal (H) and vertical (V) linear polarized waves which will cause a high pulse repetition frequency and severe range ambiguities and reduce the swath coverage relative to single and dual-polarization SAR imagery and has higher system requirements [1].

Over recent years, compact polarimetric (CP) SAR has attracted extensive attention from researchers. As an alternative for the classic FP SAR, the CP SAR can alleviate the drawbacks of the FP SAR, and can provide more target information than the single-mode and dual-mode [2]. Depending on the polarization state of its transmitting and receiving waves, there are three types of CP SAR: the $\pi/4$ mode [3], the circular transmit and liner receive (CTLR) mode [4], and the dual circular polarization (DCP) mode [5]. The $\pi/4$ mode is characterized by the transmission of a 45° linear polarization wave, and reception of the H-polarization (H-pol) and V-polarization (V-pol) wave. The CTLR mode is based on the transmission of a circular polarization wave and reception of orthogonal H-pol and V-pol. The last mode is DCP mode, where the transmission and reception wave are both circularly polarized.

In order to extract information from the CP SAR data, two types of methods were proposed [6]. The reconstruction methods introduce the traditional algorithms for processing the FP SAR data into CP SAR, which does not introduce more useful information and introduce errors [7]. Therefore, more researchers focus on the second type of methods, which directly extract information from the CP SAR data to describe the scattering mechanisms of the target.

Compact polarization decomposition is a direct way of obtaining target scattering mechanisms, in contrast to the reconstruction methods. It can effectively extract the basic scattering mechanisms (surface scattering, double-bounce scattering, and volume scattering) of different land covers. The information obtained can be used in applications such as classification and segmentation [8]. Currently, there are two different methods in CP decomposition, including the wave-dichotomy-theorem-based (WDT-based) methods [9] and model-based decomposition methods.

The WDT-based decomposition uses a series of parameters from the four-element stokes vector (SV) [2]. The most relevant parameter is m, which represents the degree of polarization (DoP). Depending on the parameter m, the received SV can be divided into two components, a fully depolarized wave and a fully polarized wave [10]. The fully depolarized part is usually considered as the volume scattering component. In order to discriminate the dominant mechanism of the remaining parts, Charbonneau *et al*. [11] proposed the well-known $m-\delta$ decomposition using the relative phase δ. Cloude *et al*. [12] presented

Manuscript received February 24, 2021; revised May 4, 2021 and August 1, 2021; accepted September 16, 2021. Date of publication September 28, 2021; date of current version October 14, 2021. This work was supported in part by the National Natural Science Foundation of China under Grant 61801015, Grant 61871413, and Grant 41801236 and in part by the Fundamental Research Funds for the Central Universities under Grant buctrc202121. (*Corresponding author: Deliang Xiang*.)

Qiang Yin, Jie Xu, and Yongsheng Zhou are with the College of Information Science and Technology, Beijing University of Chemical Technology, Beijing 100029, China (e-mail: yinq@mail.buct.edu.cn; 2019210444@mail.buct.edu.cn; zhyosh@mail.buct.edu.cn).

Deliang Xiang is with the Beijing Advanced Innovation Center for Soft Matter Science and Engineering, Beijing University of Chemical Technology, Beijing 100029, China, and also with the Interdisciplinary Research Center for Artificial Intelligence, Beijing University of Chemical Technology, Beijing 100029, China (e-mail: xiangdeliang@gmail.com).

Fan Zhang is with the College of Information Science and Technology, Beijing University of Chemical Technology, Beijing 100029, China, and also with the Interdisciplinary Research Center for Artificial Intelligence, Beijing University of Chemical Technology, Beijing 100029, China (e-mail: zhangf@mail.buct.edu.cn).

Digital Object Identifier 10.1109/JSTARS.2021.3116166

the $m-\alpha_s$ decomposition method which is applied to the CTLR model using the random volume over ground (RVoG) model. The change of α_S from 0° to 90° indicates the change of the dominant scattering mechanism from surface scattering to the volume scattering and finally to the double-bounce scattering. Similar to Cloude's approach, Guo *et al*. [13] developed a polarimetric decomposition algorithm and introduced it to the CP decomposition of the $\pi/4$ mode. Because the SVs of the $\pi/4$ mode and the CTLR mode are different, another method of equation solution is proposed. The new method gained better results than the traditional $m-\delta$ decomposition. Raney *et al*. [14] pointed out that the ellipticity parameter χ is a robust choice. The sign of χ is a clear indicator of the single and double-bounce scattering mechanisms, even if the radiated electromagnetic field is not perfectly circularly polarized. The $m-\chi$ method was proposed, and performed well in separating the surface and double-bounce scattering mechanisms. Bhattacharya *et al.* [15] proposed the $S-\Omega$ method, which takes into accounts both the transmitted and received wave ellipticities and the orientation angles. Kumar *et al.* [16] improved the $S-\Omega$ method by utilizing the degree of dominance in the scattering mechanism via the circular polarization ratio. Hou *et al.* [17] proposed a general two-stage model-based three-component HCP decomposition method by involving Arii volume scattering model to obtain closer results to the FP method.

The model-based decomposition for CP SAR, derived from the traditional Freeman–Durden three-component model-based decomposition for FP SAR, was first proposed by Guo *et al*. [18]. Under the reflection symmetry assumption, the solution process of the model is given, and the sign of $Re(\langle S_{HH}S_{VV}^{*}\rangle)$ is used as the discriminant condition for the predominance of the surface scattering or double-bounce scattering mechanism. Then, Kumar *et al*. [19] introduced the Yamaguchi volume scattering model and extended Guo's method. The improved model-based decomposition method can achieve better performance in the real CTLR mode data than before.

However, for all the above-mentioned model-based decomposition methods, there is a problem of overestimation of volume scattering (OVS) in urban areas. This is due to the fact that most decomposition methods attribute the depolarization part purely to the volume scattering mechanism and ignore the contributions of the double-bounce and surface scatterings to the depolarization [20]. The obliquely oriented buildings (OOBs) can cause considerable OVS. Due to the angle between the radar azimuth direction and the vertical wall direction of buildings, strong cross-polarization powers exist [21], making it difficult to distinguish the urban areas and natural areas. To deal with these issues. Wang *et al*. [20] concluded two ways, one is to directly reduce the scattering component by using the volume-scattering-related factor, and the other is to estimate the volume scattering component based on a reconstruction method. The first method is that the choice of parameters needs to be based on the performance of the decomposition. And the second method requires iteration for the calculation. Therefore, it is necessary to alleviate the OVS problem with a simpler and more effective way.

In this article, the following three parts are summarized to demonstrate our work.

1) A new scattering descriptor of OOBs for the CP mode is introduced to reduce the volumetric scattering in the urban areas. This descriptor, applied to both the $\pi/4$ mode and CTLR mode, performs well in the characterization for urban areas, especially for the OOBs.
2) A model-based decomposition method based on this descriptor is further proposed and this method is applicable to both the $\pi/4$ mode and CTLR mode.
3) The proposed method can reduce the negative impact of OVS and achieve satisfactory decomposition results. The Radarsat-2 quad-pol data are used to simulate the CP SAR data and to validate the proposed algorithm.

The rest of this article is organized as follows. Section II introduces the new descriptor of OOBs and the proposed decomposition method. Section III presents the decomposition results with discussions, and Section IV concludes this article.

II. Methodology

A. Eigenvalue Analysis of the CP SAR Data

For the $\pi/4$ mode and the CTLR mode, the target vector can be obtained as follows:

$$k_{\frac{\pi}{4}} = \begin{bmatrix} E_{HL} \\ E_{VL} \end{bmatrix} = \begin{bmatrix} S_{HH} & S_{HV} \\ S_{VH} & S_{VV} \end{bmatrix} \frac{1}{\sqrt{2}} \begin{bmatrix} 1 \\ \pm 1 \end{bmatrix} = \frac{1}{\sqrt{2}} \begin{bmatrix} S_{HH} \pm S_{HV} \\ S_{VH} \pm S_{VV} \end{bmatrix} \tag{1}$$

$$k_{CTLR} = \begin{bmatrix} E_{HC} \\ E_{VC} \end{bmatrix} = \begin{bmatrix} S_{HH} & S_{HV} \\ S_{VH} & S_{VV} \end{bmatrix} \frac{1}{\sqrt{2}} \begin{bmatrix} 1 \\ \pm j \end{bmatrix} = \frac{1}{\sqrt{2}} \begin{bmatrix} S_{HH} \pm jS_{HV} \\ S_{VH} \pm jS_{VV} \end{bmatrix} \tag{2}$$

where the@@ "+" sign is for +45° linear polarization and the "−" sign is for −45° linear polarization in the $\pi/4$ mode. Similarly, the "+" sign denotes left-hand circular polarization and the "−" sign is for right-hand circular polarization in the CTLR mode.

SV $S=(S_0,S_1,S_2,S_3)^T$ is a widely applied measurement for characterization of the polarization states, where the elements denote the real power measurements. The 2×2 coherency matrix of CP SAR, i.e., the second-order statistic of scattering vector, can be described by SV with the following form:

$$J_2 = \left\langle kk^H \right\rangle = \begin{bmatrix} J_{11} & J_{12} \\ J_{12}^{*} & J_{22} \end{bmatrix} = \frac{1}{2} \begin{bmatrix} S_0+S_1 & S_2-jS_3 \\ S_2+jS_3 & S_0-S_1 \end{bmatrix} \tag{3}$$

where $*$ denotes conjugate. An important parameter m , which represents DoP, can be calculated as follows:

$$m = \frac{\sqrt{S_1^2+S_2^2+S_3^2}}{S_0}. \tag{4}$$

Once we get covariance matrix, we can also calculate two non-negative real eigenvalues [9] as follows:

$$\lambda_1 = \frac{1}{2}\left(S_0 + \sqrt{S_1^2+S_2^2+S_3^2}\right) \tag{5}$$

$$\lambda_2 = \frac{1}{2}\left(S_0 - \sqrt{S_1^2 + S_2^2 + S_3^2}\right). \tag{6}$$

Similar to FP SAR, polarimetric anisotropy (A_P) for CP SAR is defined as the relative relationship between two eigenvalues. A_P is defined as follows:

$$A_P = \frac{\lambda_1 - \lambda_2}{\lambda_1 + \lambda_2} \tag{7}$$

when two eigenvalues are close, the A_P tends to 0. When the anisotropy tends to 1, it means that one of the eigenvalues is close to 1 and the other is close to 0. We can obtain m based on (5)–(7).

B. New CP Descriptor of Obliquely Oriented Buildings (D_{OOB})

Quan *et al*. [22] proposed an urban area descriptor for FP data, which successfully characterized the scattering of OOBs and modified the cross-scattering model. Inspired by this approach, we propose an eigenvalue-based descriptor based on the CP eigenvalues as follows:

$$\begin{aligned} D_{OOB} &= D_{DP} \cdot D_{RD} \cdot (1 - D_{AP}) \\ &= (\gamma \cdot S_0) \cdot I_{RV} \cdot (1 - A_P) = \frac{2\gamma^2 S_0^2 (\lambda_1 - \lambda_2)}{(\lambda_1 + \lambda_2)^2} \end{aligned} \tag{8}$$

The first part of the equation is D_{DP}, which presents the depolarization power by a cross-polarization related parameter γ multiply the total power S_0. The second part is D_{RD}, we introduce the radar vegetation index (RVI) to describe the randomness part. The last part denotes polarimetric anisotropy.

For an OOB, the cross-polarization component, which is usually linked to a depolarization component, accounts for a large proportion. In [23], an eigenvalue-based parameter γ is introduced to measure the cross-polarization component. Here, we use it to denote the depolarization part

$$\gamma = \frac{\lambda_2}{\lambda_1}. \tag{9}$$

1) When $\gamma = 0$ follows $\lambda_2 = 0$, it can be derived that ${S_0}^2 = S_1^2 + S_2^2 + S_3^2$. According to (3), we know that $\langle J_{11}\rangle \langle J_{22}\rangle = |\langle J_{12}\rangle|^2$, which is equal to $|J|^2 = 0$. So, the correlation is maximum and the receiving wave is completely polarized.
2) When $\gamma = 1$ follows $\lambda_1 = \lambda_2$, it can be derived that $S_1^2 + S_2^2 + S_3^2 = 0$, i.e., $S_1 = S_2 = S_3 = 0$. According to (3), we know that $\langle J_{12}\rangle = 0$, which makes the coherency matrix a diagonal matrix. So, the correlation is 0 and the receiving wave is completely depolarized.

RVI [24] is widely used for measuring randomness in FP SAR. Apart from the entropy, the RVI is another way of measuring randomness in the scattering process. The RVI for CP SAR is rewritten as follows:

$$I_{RV} = \frac{2\gamma \cdot S_0}{\lambda_1 + \lambda_2}. \tag{10}$$

The denominator represents the cross-polarization power, which corresponds to the λ_3 in FP SAR. For a deterministic target, the denominator is approximately 0 follows $I_{RV} = 0$. For a completely random target, $\lambda_1 \approx \lambda_2 \approx \gamma \cdot S_0$ follows $I_{RV} = 1$.

The last part denotes polarimetric anisotropy (A_P). Here, we introduce A_P in order to increase the difference between natural areas and urban areas to some extent. As shown before, A_P describes the relative relationship between eigenvalues. The A_P in natural area such as forest area is relatively higher than urban area, which makes $(1 - A_P)$ a higher value for OOBs.

C. Improved Three-Components Decomposition Method

1) The decomposition method for the CTLR mode

Cloude *et al*. [12] presented the $m - \alpha_s$ decomposition method, which is based on the RVoG model. To further improve the decomposition results, D_{OOB} is used to reduce the volume scattering component.

For the CTLR mode data, the RVoG model can be shown as follows [12]:

$$S = S_v + S_p = 2m_v \begin{bmatrix} 1 \\ 0 \\ 0 \\ 0 \end{bmatrix} + m_p \begin{bmatrix} 1 \\ \sin 2\alpha \cdot \cos\varphi \\ \pm \sin 2\alpha \cdot \sin\varphi \\ \pm \cos 2\alpha \end{bmatrix} \tag{11}$$

where S_v is the SV of the random volume scattering mechanism part and S_p is the SV of the rank-1 scattering mechanism part including the surface scattering and double-bounce scattering for the CTLR mode. m_v and m_p denote the coefficients of the volume scattering component and the rank-1 scattering component, respectively. α and φ are scattering parameters, which can be estimated by the SV elements [12]

$$\alpha = \frac{1}{2}\tan^{-1}\left(\frac{\sqrt{S_1^2 + S_2^2}}{\pm S_3}\right) \varphi = \arg\left(S_1 \pm iS_2\right). \tag{12}$$

To simplify calculations, $m_p/2, a, b, c$ are used to replace m_p, $sin2\alpha\ cos\varphi$, $\pm sin2\alpha\ sin\varphi$, $\pm cos2\alpha$. Then, four equations can be established as shown in the following:

$$\begin{cases} 2m_v + m_p = S_0 \\ m_p a = S_1 \\ m_p b = S_2 \\ m_p c = S_3 \end{cases}. \tag{13}$$

Where the constraint $a^2 + b^2 + c^2 = 1$ can be obtained at the same time.

Cloude *et al.* [12] used parameter m, i.e., the DoP to estimate m_v and m_p. The complete depolarization part is assumed to be the volume scattering part, i.e., $m_v = (1 - m)S_0$, which can result in the OVS in urban areas. Here, we decrease m_v by decreasing the value of $a^2 + b^2 + c^2$ as shown in the following:

$$\begin{cases} 2m_v + m_p = S_0 & \text{(14a)} \\ m_p a = S_1 & \text{(14b)} \\ m_p b = S_2 & \text{(14c)} \\ m_p c = S_3 & \text{(14d)} \\ a^2 + b^2 + c^2 = 1 - D_{OOB}. & \text{(14e)} \end{cases}$$

Here, $a, b,$ and c represent the intermediate variables for the solution of the equation. The urban-area-related parameter D_{OOB} is used to change the model of the rank-1 scattering mechanism, as shown in (11), so that the urban-area scattering mechanism can be better described. Here, the D_{OOB} is normalized to 0-1; thus, ensuring that the right side of (14e) is not less than 0. When the urban-area-related parameter D_{OOB} increases, the value of $a^2 + b^2 + c^2$ decreases, which leading to an increase in m_p. Based on (14a), m_v decreases at the same time, which effectively reduces the volume scattering component in urban areas.

Here are details about solving the equation.

Algorithm 1: The Equation Solution of the CTLR Mode.

1: Begin
2: Based on (14b)–(14d), we can obtain a, b, c by m_p.
3: Substitute a, b, c into (14e), and the expression of m_p is $m_p = \sqrt{(S_1^2 + S_2^2 + S_3^2)/1 - D_{OOB}}$.
4: Once we got m_p, we can get m_v by $m_v = (S_0 - m_p)/2$.
5: Both a, b and c can be represented by m_p. Set D_{OOB} to zero, and α can be obtained.
6: P_s , P_d and P_v can be obtained based on m_p , m_v and α.
7: End

According to the solution, the energy of the volume scattering and the rank-1 scattering can be got. We will then allocate m_p to the surface scattering and the double scattering depending on α in (12). The parameter α determines whether the dominant scattering mechanism is surface scattering or double scattering. Since $a^2 + b^2 + c^2 = 1$ is no longer satisfied, we set D_{OOB} to zero to calculate α. Therefore, the α is the same as Cloude's method [12]. $\alpha = 0$ corresponding to surface scattering and $\alpha = 90^\circ$ corresponding to double-bounce scattering. Therefore, $1 \pm \cos 2\alpha$ is used to express the surface and double scattering energies, respectively. The result of three-components decomposition is

$$\begin{cases} P_s = 0.5m_p(1 + \cos 2\alpha) \\ P_d = 0.5m_p(1 - \cos 2\alpha) \\ P_v = 2m_v \end{cases}. \tag{15}$$

2) The decomposition method for the π/4 mode

Guo *et al*. [13] developed a polarimetric decomposition algorithm and introduced it to the CP decomposition of the π/4 mode. We use an optimization strategy similar to the CTLR mode to reduce the negative impact of the OVS.

For the π/4 mode data, the RVoG model can be shown as follows [13]:

$$S = S_v + S_p = 2m_v \begin{bmatrix} 1 \\ 0 \\ 0.5 \\ 0 \end{bmatrix} + m_p \begin{bmatrix} 1 \\ \sin 2\alpha \cdot \cos\varphi \\ \pm \sin 2\alpha \cdot \sin\varphi \\ \pm \cos 2\alpha \end{bmatrix} \tag{16}$$

where S_v is the random volume scattering mechanism part and S_p is the rank-1 scattering mechanism part including the surface scattering and double-bounce scattering for the π/4 mode. Noted that the models for the π/4 mode are formally different from the models in the CTLR mode. Therefore, four equations have different forms as follows:

$$\begin{cases} 2m_v + m_p = S_0 \\ m_p a = S_1 \\ m_v + m_p b = S_2 \\ m_p c = S_3 \end{cases}. \tag{17}$$

The same strategy is used to reduce the volume scattering component for the π/4 mode with the following set of equations:

$$\begin{cases} 2m_v + m_p = S_0 & \text{(18a)} \\ m_p a = S_1 & \text{(18b)} \\ m_v + m_p b = S_2 & \text{(18c)} \\ m_p c = S_3 & \text{(18d)} \\ a^2 + b^2 + c^2 = 1 - D_{OOB}. & \text{(18e)} \end{cases}$$

To solve the equations, steps should be taken as shown in Algorithm 2.

Algorithm 2: The Equation Solution of the π/4 Mode.

1: Begin
2: Based on (18b) and (18d), we can use m_p to describe a, c.
3: Through (18a), the relationship between m_p and m_v can be shown as $m_v = (S_0 - m_p)/2$.
4: Based on (18c), b can be deduced as $b = (2S_2 - S_0 - m_p)/(2m_p)$.
5: As shown above, both a, b and c can be represented by m_p. Substitute a, b, c into (18e), and m_p can be obtained.
6: Once we got m_p, we can get m_v by $m_v = (S_0 - m_p)/2$.
7: Use A, B, C to replace a, b, c and set D_{OOB} to zero. m_p is recalculate, thus A, B, C, and α can be obtained.
8: P_s , P_d and P_v can be obtained based on m_p , m_v and α.
9: End

Similarly, parameter α will allocate m_p to surface scattering mechanism and double scattering mechanism. The α and φ can be estimated by the SV elements [12]

$$\alpha = \frac{1}{2}\tan^{-1}\left(\frac{\sqrt{A^2 + C^2}}{\pm B}\right) \varphi = \arg(S_1 \pm iS_3) \tag{19}$$

where A , B, and C are the special values of a, b, and c in the case when D_{OOB} is equal to 0. When D_{OOB} is zero, α is equal to the original α obtained by Guo's method [13].

Finally, the flowchart of the proposed method is shown in Fig. 1. In order to prevent the negative power, we use $1 - \mathrm{m}^2$ to limit the value of D_{OOB}.

III. Results and Discussion

In this article, the C-band Radarsat-2 FP SAR data are used to simulate the CP SAR data and validate our proposed approach. As shown in Table I, this data were obtained on April 9, 2008.

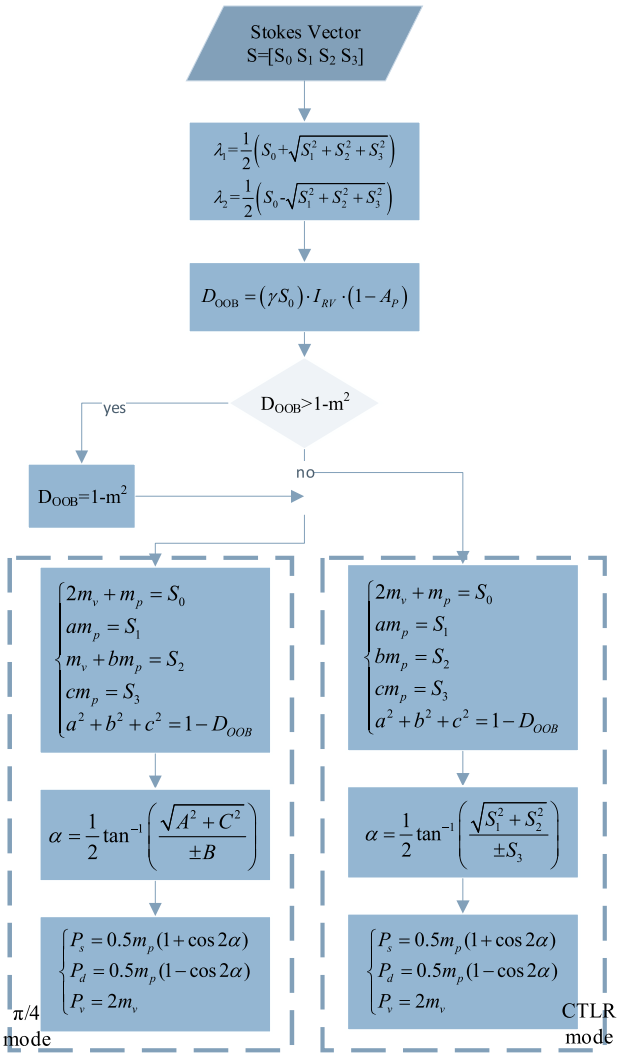

Fig. 1. Flowchart of the proposed decomposition method.

TABLE I
ACQUISITION INFORMATION ABOUT THE POLSAR DATA

Band	Date	Flight direction	Incidence angle
C	April 9, 2008	Ascending	28°

The study site is over San Francisco, USA, which includes different terrain types, such as urban areas, forests, oceans, etc. The National Land Cover Database 2008 (NLCD 2008) is used to illustrate the ground truth, as shown in Fig. 2, where the shade of red pixels indicates the density of the urban areas.

Refined Lee filter is used to decrease the speckle influence. We obtained the 2×2 coherency matrices C_2 of the CTLR mode and the $\pi/4$ mode from the 3×3 coherency matrices of FP data.

Cloude's $m-\alpha_s$ decomposition method [12] is only applicable to the CTLR mode, due to the specificity of the volume-scattering SV. Guo improved the $m-\alpha_s$ method and proposed a new model-based decomposition method that is applicable to the $\pi/4$ mode [13]. In this article, these two methods are used for comparison.

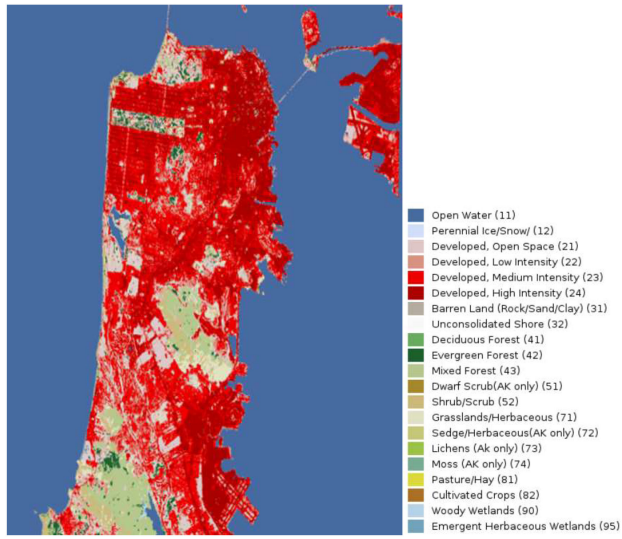

Fig. 2. Ground reference from the National Land Cover Database 2008.

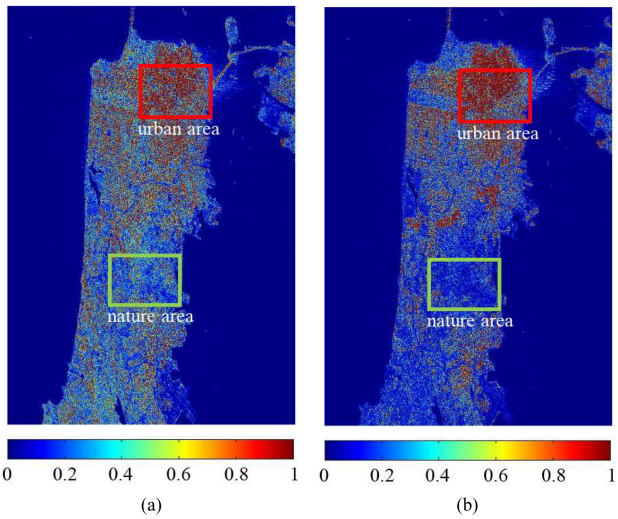

Fig. 3. Descriptor of the OOBs for (a) CTLR mode and (b) $\pi/4$ mode.

A. *Descriptor of Obliquely Oriented Buildings*

Fig. 3 illustrates the D_{OOB} of different modes. Red and green rectangular areas indicate an urban area and a natural area, respectively. As shown in Fig. 3, most of the urban areas, including the OOBs, are shown in deep red color, while the natural areas are shown in a light blue or deep blue color. Thus, D_{OOB} has the function of discriminating the urban areas from natural areas. Fig. 4 illustrates the feature histograms of the D_{OOB} for different modes. As shown in Fig. 4, the D_{OOB} among urban areas is relatively high than natural areas, for both the CTLR mode and the $\pi/4$ mode. However, the D_{OOB} of the CTLR mode obtain higher value among nature areas than the $\pi/4$ mode, as shown in Fig. 4. Because of the different scattering vectors in different modes, different λ are obtained from the eigenvalue decomposition. This leads to a smaller A_P value obtained for the CTLR mode than for the $\pi/4$ mode, and a smaller D_{OOB} value is obtained.

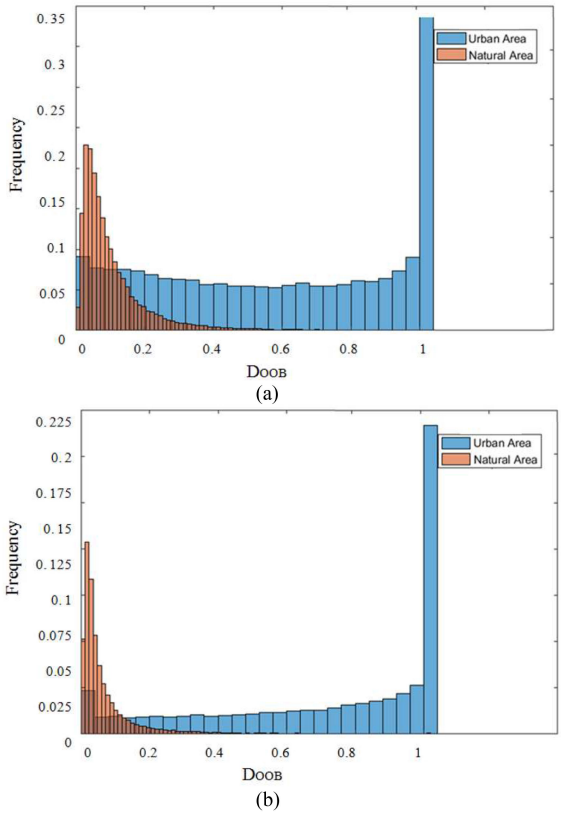

Fig. 4. Figure histograms of the D_{OOB} for (a) CTLR mode and (b) the $\pi/4$ mode.

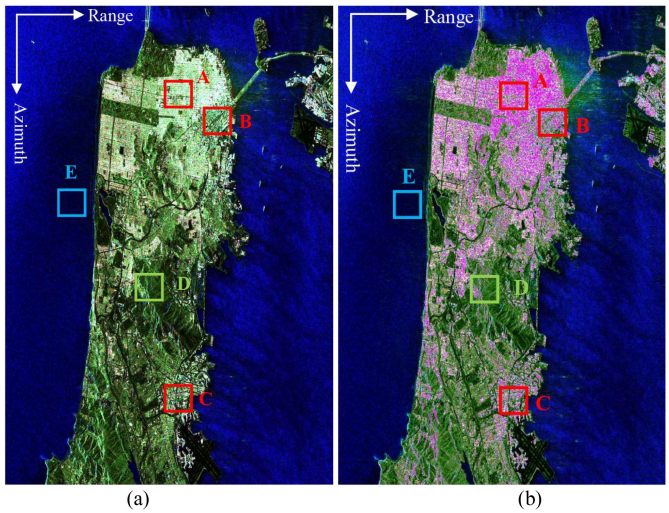

Fig. 5. Comparison of the proposed decomposition method with m-α_s decomposition method for the simulated CP SAR data of the CTLR mode over San Francisco, USA. (a) m-α_s. (b) Proposed. Red (double-bounce scattering), green (volume scattering), and blue (surface scattering).

B. Decomposition Result for the CTLR Mode

In the following, the comparison of the proposed decomposition method with the $m-\alpha_s$ decomposition method for the CTLR mode is shown in Fig. 5. The images of Fig. 5 are color-coded with P_d as red, P_v as green, and P_s as blue. For better presentation of the decomposition results, the decomposed energy is normalized to 0-1. Overall, the proposed decomposition method gains better performance than the $m-\alpha_s$ decomposition method. For the classic $m-\alpha_s$ decomposition, the urban areas, especially with large orientation angles, are colored by slight yellow and green. Meanwhile, the result of the proposed method is shown in red in most of the urban areas. The contribution of volume scattering among the urban areas is successfully reduced by applying our method.

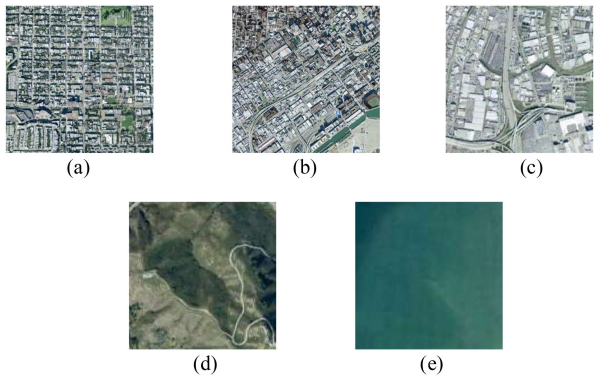

Fig. 6. Enlarged optical images of the selected patches. (a) Patch A. (b) Patch B. (c) Patch C. (d) Patch D. (e) Patch E.

Five patches with different terrain types are selected to evaluate the performance of the decomposition. The patches of A, B, and C show the OOBs with different orientation angles. The patches D and E show the forests and oceans, respectively. Fig. 6 is the enlarged optical images of selected areas. The mean power of each selected patch is illustrated in Fig. 7.

For the urban areas, the dominant scattering mechanism is double-bounce scattering. Patch A shows a density urban area with a small orientation angle. The percentages of double-bounce scattering are 37.37% and 48.94% for the $m-\alpha_s$ and the proposed method as shown in Fig. 7(a) and (f). And the percentages of volume scattering component are 26.99% and 5.74%, respectively. This result indicates that our method can elevate the double-bounce scattering and reduce the volume scattering effectively. However, the reduced volume scattering component is also allocated to surface scattering component, thus increasing the power of surface scattering. The reason is that the proposed method divides the reduced volume scattering component into the rank-1 scattering component, which is assigned to the surface scattering component and the double-bounce scattering component using the parameter α.

The terrain type of patch B is urban area with a large orientation angle, which generates cross-scattering power and can be confused with the nature area such as forests. It also contains some water areas and roads which can lead to higher surface scattering. As shown in Fig. 7(b), the percentages of P_s, P_d and P_v obtained by the $m-\alpha_s$ method are 39.19%, 36.75% and 24.06%, respectively. The volume scattering component obtained via the proposed method is reduced to 9.41% and some of them are allocated to the double-bounce scattering power and the surface scattering power, as illustrated in Fig. 7(g). Because the allocation for surface scattering and double-bounce scattering

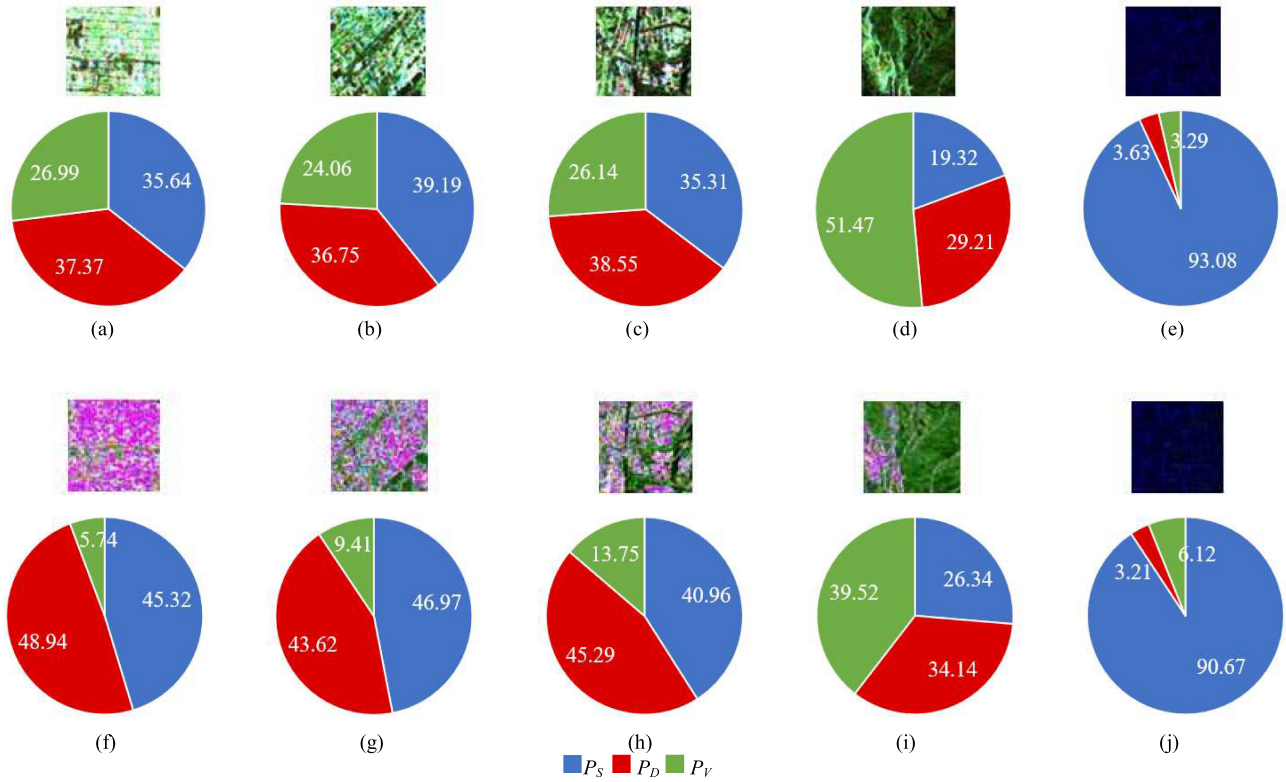

Fig. 7. Mean power statistics and enlarged images of the decomposition results obtained via the m-α_s decomposition and the proposed method. (a)–(e) m-α_s method for patches A–E. (f)–(j) Proposed method for patches A–E.

is the same as for the $m - \alpha_s$ method, surface scattering power still takes up a lot of weight.

Notably, the circularly polarized waves should not affected by the orientation of the targets [4]. However, the problem of OVS due to the orientation angle does exist during the study of the CTLR mode. We considered that the process of simulation, which introduces an additional linear polarization component from the real FP data to the CP data, results in the problem of building orientation.

For patch C, the density of buildings is relatively low and the alignment is irregular in different directions. The double-bounce scattering is the dominate part. According to Fig. 7(c) and (h), P_d contributes 38.55% and 45.29% for the $m - \alpha_s$ and the proposed method, respectively. And the percentages of volume scattering are 26.14% and 13.75%, which is another proof of the effectiveness of our method.

Nature areas in patch D are mixed forests, and the dominant scattering is volume scattering. The percentages of P_v are 51.47% and 39.52% as shown in Fig. 7(d). Because the D_{OOB} of the CTLR mode obtains a higher value among nature area than that of the $\pi/4$ mode, some volume scattering components in those areas are assigned to other scattering components, which leads to the decrease of volume scattering power. However, the volume scattering is still the dominant scattering mechanism for the result of our proposed method, according to Fig. 7(i).

For the ocean area, the dominant scattering mechanism is surface scattering. The percentages contribution of P_s are 93.08% and 90.67% for the $m - \alpha_s$ and the proposed method as shown in Fig. 7(e) and (j). The value of D_{OOB} for the ocean area is approximately 0, so the proposed method has minimal effect on the results.

TABLE II
PERCENTAGES OF DOMINANT SCATTERING COMPONENTS(%)

	Proposed method			m-α_s method		
patch	S	D	V	S	D	V
A	41.45	55.94	2.62	17.10	31.69	51.21
B	39.00	38.68	22.32	20.01	23.02	56.97
C	23.96	37.11	38.93	16.06	29.44	54.50
D	8.65	18.54	72.81	4.99	18.61	76.40
E	99.44	0.04	0.52	99.78	0.07	0.15

To evaluate the effectiveness of different decomposition methods, a pixel-by-pixel classification experiment is presented in Table II. Based on the power of each scattering component, the dominant scattering mechanism is selected for each pixel. The percentage of pixels with different scattering mechanisms is calculated for each selected area.

For patch A, the percentages of pixels which double-bounce scattering dominants raise from 31.69% to 55.94%. And the percentages of volume-scattering-dominant pixels decrease from 51.21% to 2.62%. The statistics shows that the proposed method has a big influence to urban areas with small orientation angles, and increase the double-bounce scattering percentage to 55.94%.

For patch B, the percentages of pixels which double-bounce scattering dominants raise from 23.02% to 38.68% by applying

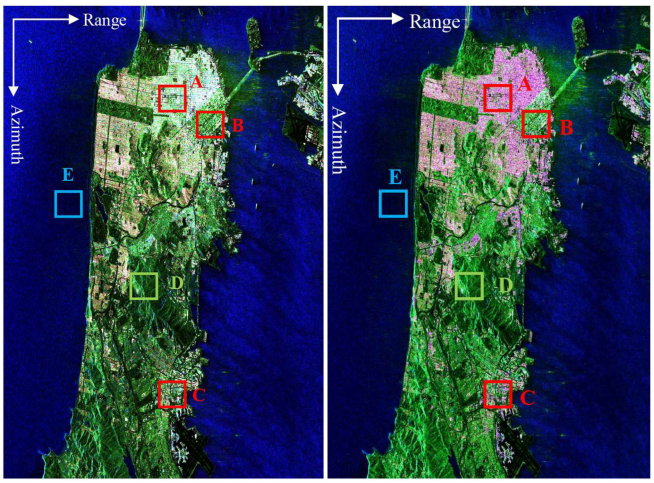

(a) (b)

Fig. 8. Comparison of the proposed decomposition method with Guo's decomposition method for the simulated CP SAR data of the $\pi/4$ mode over San Francisco, USA. (a) Guo's. (b) Proposed. Red (double-bounce scattering), green (volume scattering), and blue (surface scattering).

the proposed method. And the percentages of volume-scattering-dominant pixels decrease from 56.97% to 22.32%. The proposed method can also decrease a large proportion of the volume scattering pixels and reduce the misjudge of urban areas with large orientation angles.

As for patch C, the percentages of pixels which double-bounce scattering dominants raise from 29.44% to 37.11%. And the percentages of volume-scattering-dominant pixels decrease from 54.5% to 38.93%. Because the patch C has a lower building density than paths A and B, the number of volume-scattering-dominant pixels is less than in patches A and B.

Although the double-bounce scattering pixels increase a large proportion in urban areas, the natural areas are less affected by the proposed method. For patch D, which volume scattering dominants, the percentages of pixels for volume scattering is 76.4% and 72.81% for the proposed method and the $m - \alpha_s$, respectively. And for patch E, which surface scattering dominants, the percentages of pixels for surface scattering are 99.78% and 99.44%.

Overall, the proposed decomposition method of the CTLR mode effectively improves the double-bounce scattering power in urban areas (including areas with large orientation angles), but the surface scattering power is greatly increased at the same time. Considering that the roofs of the building and roads in streets generate strong surface scattering component, the result is acceptable. With the decrease of volume scattering power, more pixels in urban areas are distinguished from natural areas, improving the quality of the decomposition results.

C. Decomposition Result for the $\pi/4$ Mode

The comparison of the proposed decomposition method with Guo's decomposition method for the $\pi/4$ mode is shown in Fig. 8.

In general, the proposed decomposition method gains better performance than Guo's decomposition method. For Guo's decomposition method, most of the urban areas are colored by slight yellow and green. At the same time, the result of the proposed method shows red in most of the urban areas and obtains a better result. The contribution of volume scattering among the urban areas is successfully reduced by applying our method, similarly to the CTLR mode.

The same five patches were selected to evaluate the performance of the decomposition.

The terrain type of Patch A is a high-density urban area with a small orientation angle. As shown in Fig. 9(a) and (f), the percentages of double-bounce scattering are 33.62% and 36.85% for Guo's method and the proposed method. And the percentages of volume scattering component are 29.6% and 18.37%, respectively. For the $\pi/4$ mode, the proposed method can also elevate the double-bounce scattering component and reduce the volume scattering component effectively.

The terrain type of patch B is urban area with a large orientation angle. A large proportion of cross-scattering power generates and can be confused with nature area such as forests. It also contains some water areas and roads which can lead to a high surface scattering. As shown in Fig. 9(b), the percentages of P_s, P_d, and P_v obtained by Guo's method are 42.46%, 27.94%, and 29.6%, respectively. Similar to the results of [13], the volume scattering power is higher than the $\pi/4$ mode. The volume scattering component obtained via the proposed method is reduced to 18.37%, and some of which are allocated to the double-bounce scattering power, as illustrated in Fig. 9(g). There exists the same problem as the decomposition results of the CTLR mode, surface scattering power is elevated to 47.03% by applying the proposed method, because of the parameter α used to assign surface scattering component and double-bounce scattering component.

For patch C, the density of buildings is relatively low and the alignment is irregular in different directions. Double-bounce scattering is the dominate part. According to Fig. 9(c) and (h), P_d contributes 36.76% and 47.75% for Guo's and the proposed method, respectively. And the percentages of volume scattering are 28.35% and 14.69%, which can also show the effectiveness of the proposed method.

As for patch D, where the terrain types are mixed forests, and the dominant scattering is volume scattering. The percentages of P_v are 58.56% and 54.66% as shown in Fig. 9(d). Different from the result of the CTLR mode, the value of D_{OOB} for the $\pi/4$ mode is relatively lower among nature areas, so the volume scattering is almost unchanged for the result of our proposed method, according to Fig. 9(i).

For the ocean area, the dominant scattering mechanism is surface scattering. The percentages contribution of P_s are 90.58% and 90.62% for Guo's and the proposed method as shown in Fig. 9(e) and (j). The value of D_{OOB} for the ocean area is approximately 0, so the proposed method does not change the scattering mechanism of natural areas for the $\pi/4$ mode.

The same pixel-by-pixel classification experiment is done for the $\pi/4$ mode, the results are listed in Table III. Based on the

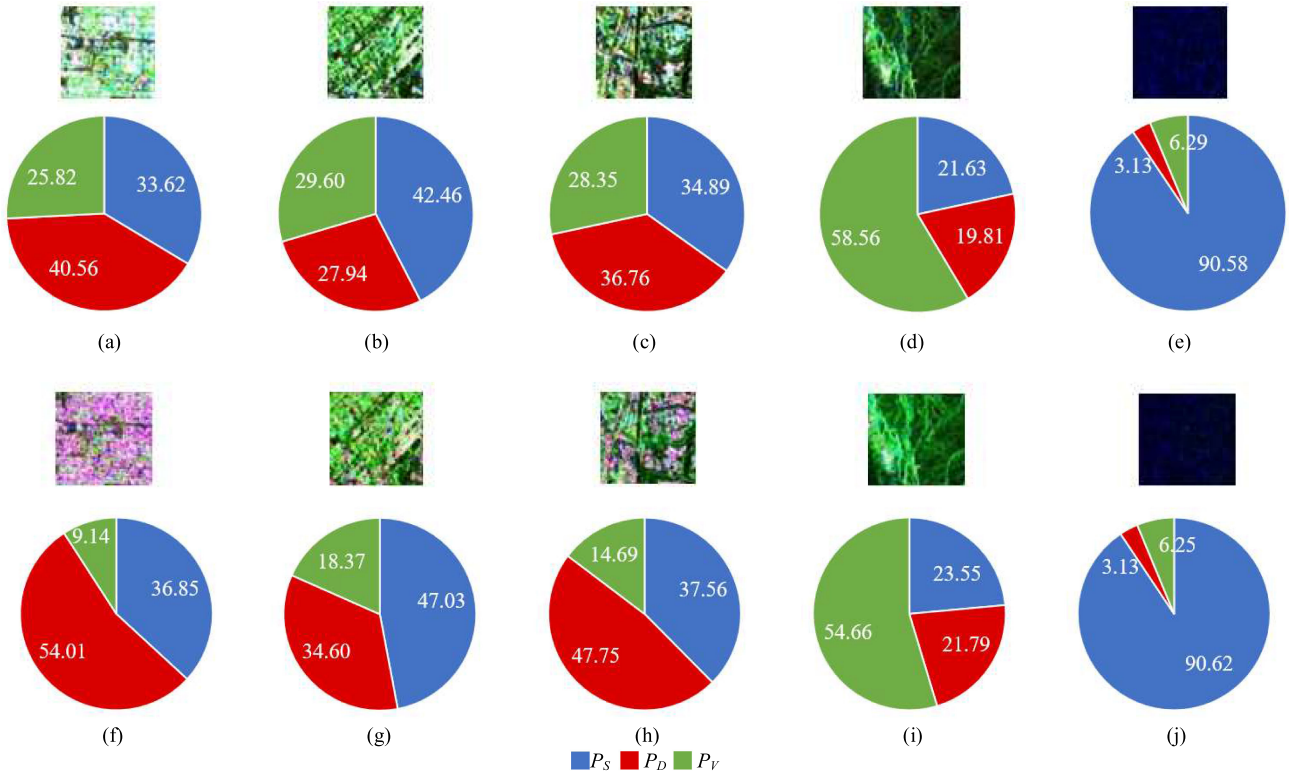

Fig. 9. Mean power statistics and enlarged images of the decomposition results obtained via Guo's decomposition and the proposed method. (a)–(e) Guo's method for patches A–E. (f)–(j) Proposed method for patches A–E.

TABLE III
PERCENTAGES OF DOMINANT SCATTERING COMPONENTS(%)

	Proposed method			Guo's method		
patch	S	D	V	S	D	V
A	21.20	68.28	10.52	19.28	31.49	49.23
B	20.58	40.19	39.23	11.75	15.67	72.58
C	18.26	46.31	35.43	15.43	25.32	59.25
D	10.43	8.16	81.41	8.93	5.49	85.58
E	98.94	0.08	0.98	98.91	0.08	1.01

Fig. 10. Enlarged optical images of selected patches. (a) Patch A: Urban area. (b) Patch B: Natural area.

power of each scattering component, the dominant scattering mechanism is selected for each pixel. The percentage of pixels with different scattering mechanisms is calculated for each selected area.

For patch A, the percentages of pixels which double-bounce scattering dominants raise from 31.49% to 68.28%. And the percentages of volume-scattering-dominant pixels decrease from 49.23% to 10.52%. The statistics shows that the proposed method has a big influence to urban areas with small orientation angles, and remarkably increase the percentage of double-bounce scattering pixels.

For patch B, the percentages of pixels which double-bounce scattering dominants raise from 15.67% to 40.19%. And the percentages of volume-scattering-dominant pixels decrease from 72.58% to 39.23% by applying our method. The proposed method can also decrease a large proportion of the volume scattering pixels and reduce the misjudge of urban areas with large orientation angles.

As for patch C, the percentages of pixels which double-bounce scattering dominants raise from 25.32% to 46.31% by applying our method. And the percentages of volume-scattering-dominant pixels decrease from 59.25% to 35.43%.

Although the double-bounce scattering pixels increase a large proportion in urban areas, the natural areas are less affected by the proposed method. For patch D, which volume scattering dominants, the percentages of pixels for volume scattering are 85.58% and 81.41%, respectively. And for patch E, which surface scattering dominants, the percentages of pixels for surface scattering are 98.91% and 98.94%.

Overall, the proposed decomposition method of the $\pi/4$ mode gained a better result than the CTLR mode. The double-bounce scattering power is remarkably increased and the scattering power of natural areas is little affected.

Fig. 11. Decomposition result of the proposed decomposition method and Cloude's decomposition method of the CTLR mode over Rennes, France. (a) D_{OOB} for the CTLR mode. (b) Cloude's. (c) Proposed. Red (double-bounce scattering), green (volume scattering), and blue (surface scattering).

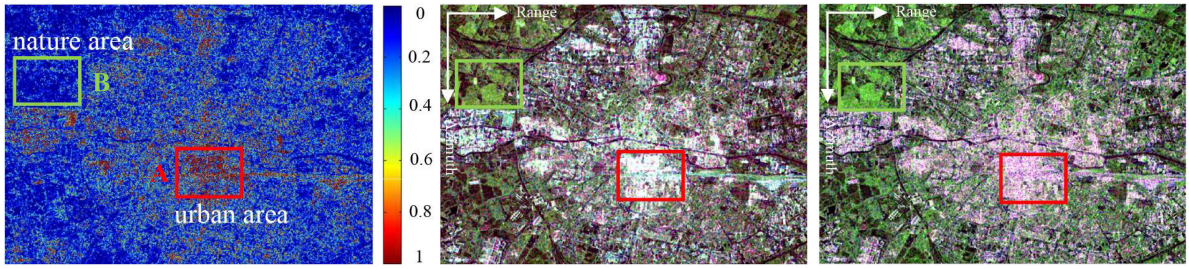

Fig. 12. Decomposition result of the proposed decomposition method and Guo's decomposition method of the $\pi/4$ mode over Rennes, France. (a) D_{OOB} for the CTLR mode. (b) Guo's. (c) Proposed. Red (double-bounce scattering), green (volume scattering), and blue (surface scattering).

D. Further Inspection on GF-3 Data

To further evaluate the effectiveness of the proposed decomposition method, the C-band GF-3 FP data are used to simulate CP data. The image size is 1780×1250 pixels, and the spatial resolution is 8 m × 8 m. This data were obtained on January 3, 2017. The study site is over Rennes, France, which contains dense urban areas and natural areas.

The decomposition results for the CTLR mode and the $\pi/4$ mode are shown in Figs. 11 and 12, respectively. Two areas are denoted on the image to show the results of the different terrain types. The enlarge optical images of the selected areas are shown in Fig. 10.

As shown in Fig. 10(a), there are buildings of different orientation angles. Both the CTLR mode and the $\pi/4$ mode obtain high D_{OOB} values, which are shown in deep red in Figs. 11(a) and 12(a). The result of Cloude's method is colored green and light yellow in the red square area in Fig. 11(b). This area has not only a part of natural areas such as grass and trees, but also various buildings in different orientation angle. This results in a relatively high level of all three scattering mechanisms at the same time, which appear as bright yellow or white in the pseudo-color image. With the improvement of the method by D_{OOB}, the OOBs are shown in red among urban areas in Fig. 11(c). Similar results were obtained for the $\pi/4$ mode in Fig. 12(b) and (c).

As for natural areas in Fig. 10(b), fields and vegetation dominate. Both the CTLR mode and the $\pi/4$ mode obtain low D_{OOB} values, which are shown in deep blue in Figs. 11(a) and 12(a). Because of the limited data we obtained, the optical images shown in Fig. 10 were acquired in September 2018. Natural area crops were abundant at the time of GF-3 data acquisition. So, the volume scattering component and the double-bounce scattering component are higher than expected, which makes the D_{OOB} not as low as expected in natural areas. Therefore, a portion of the volume scattering component for this area is converted into the double-bounced scattering component and the surface scattering component. Overall, the proposed method does not change the scattering mechanism of the original method in the natural areas.

TABLE IV
SCATTERING POWER CONTRIBUTION OVER RENNES (%)

		Proposed method			m-α_s method		
mode	patch	S	D	V	S	D	V
CTLR	A	38.01	38.70	23.29	33.69	31.47	34.84
	B	24.29	37.82	37.89	23.81	36.95	39.24
$\pi/4$	A	35.42	39.20	25.38	31.74	31.86	36.40
	B	37.36	37.21	25.43	36.46	36.31	27.23

The scattering power contribution for the $\pi/4$ mode and the CTLR mode are shown in Table IV to validate the proposed method.

E. Compared With the Model-Based Methods for the CTLR Mode

Three methods are chosen for comparison, Wang's method [20], the three-component scattering model (HTM) [19], and the general two-stage model-based decomposition method (GTM) [17]. These methods are only applicable to CTLR mode. Fig. 13 shows the pseudo-color-coded images of four methods.

The scattering power contribution for different methods is shown in Table V to validate the proposed method.

TABLE V
SCATTERING POWER CONTRIBUTION OVER SAN FRANCISCO (%)

	Proposed method			GTM			HTM			Wang's		
patch	S	D	V	S	D	V	S	D	V	S	D	V
A	45.32	48.94	5.74	23.42	47.83	28.75	23.58	46.84	29.58	30.17	40.13	29.7
B	46.97	43.62	9.41	15.83	61.25	22.92	14.58	60.61	24.81	24.04	48.71	27.25
C	40.96	45.29	13.75	25.27	46.95	27.78	24.63	46.56	28.82	30.04	40.70	29.26
D	26.34	34.14	39.52	28.22	20.76	51.02	29.85	23.76	46.39	34.65	31.46	33.89
E	90.67	3.21	6.12	95.05	2.97	1.98	96.27	0.77	2.96	83.20	5.19	11.61

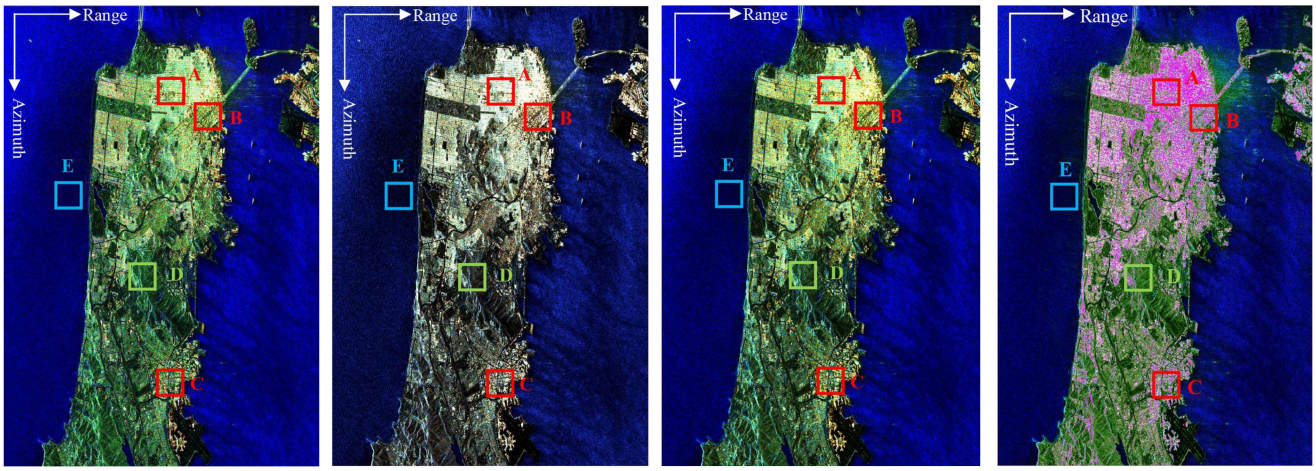

Fig. 13. Comparison with the model-based methods for the CTLR mode. (a) Wang's. (b) HTM. (c) GTM. (d) Proposed. Red (double-bounce scattering), green (volume scattering), and blue (surface scattering).

Overall, the proposed method gained better performance in reducing the volume scattering component in urban areas than recent model-based decomposition methods. The reason is that we focus more on directly reduce the volume scattering component among the urban areas depend on the descriptor D_{OOB}, the advantage of this idea is that it can greatly enhance double-bounce scattering component among the urban areas, which can help the process of classification. However, the disadvantage is that the surface scattering component increases at the same time.

IV. CONCLUSION

In this article, a model-based decomposition method for CP SAR is proposed. A new descriptor of OOBs is introduced based on the eigenvalues of the CP SAR data. This descriptor can effectively describe urban areas with different orientation angles and distinguish the buildings from natural areas. The improved model-based decomposition method based on this descriptor is proposed to reduce the OVS problem. The proposed decomposition method can be applied in both the $\pi/4$ mode and the CTLR mode, but the $\pi/4$ mode gains better performance. According to the result obtain via the proposed method, volume scattering component is reduced and double-bounce scattering component is increased in different types of urban areas. With the growth of the double-bounce scattering component, the surface scattering component grows. However, it does not affect the determination of the dominate scattering mechanism. For the natural areas such as forests and oceans, the scattering mechanisms are little affected.

In conclusion, the proposed decomposition method can overcome the OVS problem, and reduce the ambiguity of the scattering mechanism of the urban areas.

REFERENCES

[1] R. K. Raney, A. Freeman, and R. L. Jordan, "Improved range ambiguity performance in quad-pol SAR," *IEEE Trans. Geosci. Remote Sens.*, vol. 50, no. 2, pp. 349–356, Feb. 2012.
[2] R. K. Raney, "Dual-polarized SAR and stokes parameters," *IEEE Geosci. Remote Sens. Lett.*, vol. 3, no. 3, pp. 317–319, Jul. 2006.
[3] J. Souyris, P. Imbo, R. Fjortoft, S. Mingot, and J.-S. Lee, "Compact polarimetry based on symmetry properties of geophysical media: The pi/4 mode," *IEEE Trans. Geosci. Remote Sens.*, vol. 43, no. 3, pp. 634–646, Mar. 2005.
[4] R. K. Raney, "Hybrid-polarity SAR architecture," *IEEE Trans. Geosci. Remote Sens.*, vol. 45, no. 11, pp. 3397–3404, Nov. 2007.
[5] N. Stacy and M. Preiss, "Compact polarimetric analysis of X-band SAR data[C]," in *Proc. 6th Eur. Conf. Synthetic Aperture Radar*, Dresden, Germany, pp. 1–4, 2006.
[6] L. Xu *et al.*, "Progress in the processing and application of compact polarimetric SAR," *J. Radars*, vol. 9, no. 1, pp. 55–72, 2020.
[7] A. Reigber, M. Neumann, L. Ferro-Famil, M. Jager, and P. Prats, "Multi-baseline coherence optimisation in partial and compact polarimetric modes," in *Proc. IEEE Int. Geosci. Remote Sens. Symp.*, Boston, MA, USA, 2008, pp. II–597–II–600.
[8] X. Sun, B. Wang, Z. Wang, H. Li, H. Li, and K. Fu, "Research progress on few-shot learning for remote sensing image interpretation," *IEEE J. Sel. Topics Appl. Earth Observ. Remote Sens.*, vol. 14, no. 1939-1404, pp. 2387–2402, Jan. 2021.
[9] J.-S. Lee, E. Pottier, and B. J. Thompson, *Polarimetric Radar Imaging*. Boca Raton, FL, USA: CRC Press, 2009, pp. 47–51.

[10] R. K. Raney, "Comparing compact and quadrature polarimetric SAR performance," *IEEE Geosci. Remote Sens. Lett.*, vol. 13, no. 6, pp. 861–864, Jun. 2016.
[11] F. J. Charbonneau *et al.*, "Compact polarimetry overview and applications assessment," *Can. J. Remote Sens.*, vol. 36, Suppl. 2, pp. S298–S315, 2010.
[12] S. R. Cloude, D. G. Goodenough, and H. Chen, "Compact decomposition theory," *IEEE Geosci. Remote Sens. Lett.*, vol. 9, no. 1, pp. 28–32, Jan. 2012.
[13] S. Guo, Y. Li, and W. Hong, "Model-based target decomposition with the $\pi/4$ mode compact polarimetry data," *Sci. China Inf. Sci.*, vol. 59, no. 6, pp. 185–194, Jun. 2016.
[14] R. K. Raney, J. T. S. Cahill, G. W. Patterson, and D. B. J. Bussey, "The *m*-chi decomposition of hybrid dual-polarimetric radar data with application to lunar craters," *J. Geophysical Res., Planets*, vol. 117, E00H21, May 2012.
[15] A. Bhattacharya, S. De, A. Muhuri, M. Surendar, G. Venkataraman, and A. K. Das, "A new compact polarimetric SAR decomposition technique," *Remote Sens. Lett.*, vol. 6, no. 12, pp. 914–923, 2015.
[16] V. Kumar, D. Mandal, A. Bhattacharya, and Y. S. Rao, "Crop characterization using an improved scattering power decomposition technique for compact polarimetric SAR data," *Int. J. Appl. Earth Observ. Geoinf.*, vol. 88, 2020, Art. no. 102052.
[17] W. Hou, F. Zhao, X. Liu, and R. Y. Wang, "General two-stage model-based three-component hybrid compact polarimetric SAR decomposition method," *IEEE J. Sel. Topics Appl. Earth Observ. Remote Sens.*, vol. 14, pp. 4647–4660, Mar. 2021.
[18] R. Guo, W. He, S. Zhang, B. Zang, and M. Xing, "Analysis of three-component decomposition to compact polarimetric synthetic aperture radar," *IET Radar, Sonar Navigation*, vol. 8, no. 6, pp. 685–691, 2014.
[19] A. Kumar, A. Das, and R. K. Panigrahi, "Hybrid-pol based three-component scattering model for analysis of RISAT data," *IEEE J. Sel. Topics Appl. Earth Observ. Remote Sens.*, vol. 10, no. 12, pp. 5155–5162, Dec. 2017.
[20] H. Wang, Z. Zhou, J. Turnbull, Q. Song, and F. Qi, "Three-component decomposition based on stokes vector for compact polarimetric SAR," *Sensors*, vol. 15, no. 9, pp. 24087–24108, 2015.
[21] S. Quan, B. Xiong, D. Xiang, C. Hu, and G. Kuang, "Scattering characterization of obliquely oriented buildings from PolSAR data using eigenvalue-related model," *Remote Sens.*, vol. 11, no. 5, p. 581, 2019.
[22] S. Quan, B. Xiong, D. Xiang, L. Zhao, S. Zhang, and G. Kuang, "Eigenvalue-based urban area extraction using polarimetric SAR data," *IEEE J. Sel. Topics Appl. Earth Observ. Remote Sens.*, vol. 11, no. 2, pp. 458–471, Feb. 2018.
[23] M. M. Espeseth, C. Brekke, and S. N. Anfinsen, "Hybrid-polarity and reconstruction methods for sea ice with L- and C-band SAR," *IEEE Geosci. Remote Sens. Lett.*, vol. 13, no. 3, pp. 467–471, Mar. 2016.
[24] J. J. van Zyl and Y. Kim, *Synthetic Aperture Radar Polarimetry*. Pasadena, CA, USA: Wiley, 2011.

Qiang Yin (Member, IEEE) received the B.S. degree in electronic and information engineering from Beijing University of Chemical Technology, Beijing, China, in 2004, and the M.S. and Ph.D. degrees in signal and information processing from the Institute of Electronics, Chinese Academy of Science, Beijing, China, in 2008 and 2016, respectively.

From 2008 to 2013, she was a Research Assistant with the Institute of Electronics, Chinese Academy of Sciences. From 2014 to 2015, she was a Research Fellow with the European Space Agency, Roma, Italy. She is currently an Associate Professor with the College of Information Science and Technology, Beijing University of Chemical Technology. Her research interests include polarimetric/polarimetric interferometric synthetic aperture radar processing and applications.

Jie Xu received the B.E. degree in electronic and information engineering in 2019 from Beijing University of Chemical Technology, Beijing, China, where she is currently working toward the M.S. degree in control engineering.

Her research interests include the polarimetric SAR image processing and applications.

Deliang Xiang (Member, IEEE) received the B.S. degree in remote sensing science and technology from Wuhan University, Wuhan, China, in 2010, the M.S. degree in photogrammetry and remote sensing from the National University of Defense Technology, Changsha, China, in 2012, and the Ph.D. degree in geoinformatics from the KTH Royal Institute of Technology, Stockholm, Sweden, in 2016.

In 2019, he was awarded a Humboldt Research Fellowship. Since 2020, he has been a Full Professor with Interdisciplinary Research Center for Artificial Intelligence, Beijing University of Chemical Technology, Beijing, China. His research interests include urban remote sensing, synthetic aperture radar (SAR)/polarimetric SAR image processing, artificial intelligence, and pattern recognition.

Dr. Xiang serves as a Reviewer for the *Remote Sensing of Environment*, the *ISPRS Journal of Photogrammetry and Remote Sensing*, the IEEE JOURNAL OF SELECTED TOPICS IN APPLIED EARTH OBSERVATIONS AND REMOTE SENSING, the IEEE GEOSCIENCE AND REMOTE SENSING LETTERS, and several other international journals in the remote sensing field.

Yongsheng Zhou (Member, IEEE) received the B.E. degree in communication engineering from Beijing Information Science and Technology University, Beijing, China, in 2005, and the Ph.D. degree in signal and information processing from the Institute of Electronics, Chinese Academy of Sciences, Beijing, China, in 2010.

He is currently a Professor of Electronic and Information Engineering with the College of Information Science and Technology, Beijing University of Chemical Technology, Beijing, China. His general research interests lie in target detection and recognition from microwave remotely sensed image, digital signal and image processing, etc.

Fan Zhang (Senior Member, IEEE) received the B.E. degree in communication engineering from Civil Aviation University of China, Tianjin, China, in 2002, the M.S. degree in signal and information processing from Beihang University, Beijing, China, in 2005, and the Ph.D. degree in signal and information processing from the Institute of Electronics, Chinese Academy of Sciences, Beijing, China, in 2008.

He is currently a Full Professor of Electronic and Information Engineering with the College of Information Science and Technology, and the Interdisciplinary Research Center for Artificial Intelligence, Beijing University of Chemical Technology, Beijing, China. His research interests are remote sensing image processing, high-performance computing, and artificial intelligence.

Dr. Zhang is currently an Associate Editor for the IEEE ACCESS and a Reviewer for the IEEE TRANSACTIONS ON GEOSCIENCE AND REMOTE SENSING, the IEEE JOURNAL OF SELECTED TOPICS IN APPLIED EARTH OBSERVATIONS AND REMOTE SENSING, and the IEEE GEOSCIENCE AND REMOTE SENSING LETTERS, and the *Journal of Radars*.